Latitudinal distribution of reactive nitrogen in the free troposphere over the Pacific Ocean in late winter/early spring

JOURNAL OF GEOPHYSICAL RESEARCH, VOL. 103, NO. D21, PAGES 28,237–28,246, NOVEMBER 20, 1998

Latitudinal distribution of reactive nitrogen in the free troposphere over the Pacific Ocean in late winter/early spring

H. B. Singh,[1] W. Viezee,[1] Y. Chen,[1] A. N. Thakur,[1] Y. Kondo,[2] R. W. Talbot,[3] G. L. Gregory,[4] G. W. Sachse,[4] D. R. Blake,[5] J. D. Bradshaw,[6,7] Y. Wang,[8] and D. J. Jacob[8]

Abstract. The late winter/early spring (February/March, 1994) measurements of Pacific Exploratory Mission-West (PEM-W) B have been analyzed to show latitudinal distributions (45°N to 10°S) of the mixing ratios of reactive nitrogen species (NO, peroxyacetylnitrate (PAN), HNO_3, and NO_y), ozone, and chemical tracers (CO, NMHCs, acetone, and C_2Cl_4) with a focus on the upper troposphere. Mixing ratios of all species are relatively low in the warm tropical and subtropical air south of the polar jetstream (≈28°N) but increase sharply with latitude in the cold polar air north of the jetstream. Noteworthy is the continuous increase in reservoir species (PAN and HNO_3) and the simultaneous decrease in NO_x toward the northern midlatitudes. The Harvard global three-dimensional model of tropospheric chemistry has been used to compare these observations with predictions. In the upper troposphere the magnitude and distribution of measured NO_y and PAN as a function of latitude is well represented by this model, while NO_x (measured NO + model calculated NO_2) is underpredicted, especially in the tropics. Unlike several previous studies, where model-predicted HNO_3 exceeded observations by as much as a factor of 10, the present data/model comparison is improved to within a factor of 2. The predicted upper tropospheric HNO_3 is generally below or near measured values, and there is little need to invoke particle reactions as a means of removing or recycling HNO_3. Comparison between measured NO_y and the sum of its three main constituents (PAN + NO_x + HNO_3) on average show a small mean shortfall (<15%). This shortfall could be attributed to the presence of known but unmeasured species (e.g., peroxynitric acid and alkyl nitrates) as well as to instrument errors.

1. Introduction

Pacific Exploratory Mission-West (PEM-W) B was an airborne experiment designed to study the chemistry of the troposphere over the western Pacific Ocean during the winter and early spring season (February-March) of 1994. A total of 16 flights each averaging ~8 hours in duration focused on studying the impact of Asian outflow on the composition and chemistry of the Pacific troposphere. There were additional opportunities to study the troposphere and the stratosphere under largely unperturbed conditions. The airborne missions covered tropical, subtropical, and polar air masses and originated from Guam, Hong Kong, and Yokota, Japan. An overview of the PEM-W B instrumentation, experimental design, and meteorology have been provided by *Hoell et al.* [1997] and *Merrill et al.* [1997] as well as by individual investigators in the special PEM-W B issue of *Journal of Geophysical Research* (*102*(D23), 1997). This paper presents further analyses of data collected by the NASA DC-8 research aircraft during PEM-W B and compares measured and modeled latitudinal distributions of selected reactive nitrogen species (NO, HNO_3, peroxyacetylnitrate (PAN), and NO_y) and ozone (O_3) in the upper troposphere (6–12 km). The present manuscript complements other aspects of atmospheric composition and chemistry based on the PEM-W B data that have recently been published [*Kondo et al.*, 1997a; *Koike et al.*, 1997; *Thompson et al.*, 1997].

2. Data Processing and Model Application

In this manuscript we will not provide details of measurement techniques as these have appeared in previous publications (*Journal of Geophysical Research*, *102*(D23), 1997, and references therein). It is noted, however, that NO and NO_y in PEM-W B were measured by two separate investigators (Nagoya University and Georgia Institute of Technology (GIT)) using independent techniques (chemiluminescence and laser-induced fluorescence (LIF)). In both cases, NO_y was measured by catalytically converting it to NO on the surface of a heated gold tube with the addition of CO. While NO levels

[1]Earth Science Division, NASA Ames Research Center, Moffett Field, California.
[2]Solar Terrestrial Environment Laboratory, Nagoya University, Toyokawa, Japan.
[3]Institute for the Study of Earth, Oceans, and Space, University of New Hampshire, Durham.
[4]Earth Science Division, NASA Langley Research Center, Hampton, Virginia.
[5]Department of Chemistry, University of California, Irvine.
[6]School of Atmospheric Sciences, Georgia Institute of Technology, Atlanta.
[7]Deceased June 16, 1997.
[8]Department of Earth and Planetary Sciences, Harvard University, Cambridge, Massachusetts.

Paper number 98JD01891.
0148-0227/98/98JD-01891$09.00

Table 1. Reactive Nitrogen Budgets and Partitioning Based on Pacific Exploratory Mission-West (PEM-W) B Measurements at Midlatitudes (30°–45°N) and the Subtropics (10°–30°N)

Latitude, °N	Altitude, km	PAN/NO_y,* ppt/ppt	HNO_3/NO_y,* ppt/ppt	NO_x/NO_y,* ppt/ppt	NO_{y_i}/NO_y,* ppt/ppt	NO_y-NO_{y_i},* ppt
30–45	6–12 (UT)	0.43 ± 0.19 (0.48, 20)	0.34 ± 0.20 (0.29, 19)	0.08 ± 0.08 (0.05, 17)	0.86 ± 0.21 (0.83, 16)	106.1 ± 133.3 (83.6, 16)
30–45	3–6 (MT)	0.56 ± 0.13 (0.54, 10)	0.22 ± 0.09 (0.24, 10)	0.04 ± 0.02 (0.04, 6)	0.83 ± 0.17 (0.84, 6)	126.5 ± 135.4 (101.6, 6)
30–45	0–3 (LT)	0.65 ± 0.18 (0.64, 9)	0.21 ± 0.06 (0.16, 9)	0.08 ± 0.05 (0.09, 8)	0.98 ± 0.17 (1.08, 8)	26.1 ± 182.4 (−63.4, 8)
10–30	6–12 (UT)	0.26 ± 0.14 (0.22, 30)	0.44 ± 0.22 (0.36, 33)	0.22 ± 0.09 (0.22, 29)	0.89 ± 0.22 (0.80, 26)	59.2 ± 80.2 (76.7, 26)
10–30	3–6 (MT)	0.30 ± 0.19 (0.35, 17)	0.44 ± 0.31 (0.35, 19)	0.13 ± 0.04 (0.14, 16)	0.84 ± 0.27 (0.75, 14)	95.3 ± 138.6 (94.2, 14)
10–30	0–3 (LT)	0.32 ± 0.23 (0.38, 16)	0.45 ± 0.34 (0.43, 17)	0.27 ± 0.41 (0.17, 15)	0.94 ± 0.22 (0.92, 14)	95.2 ± 136.7 (76.7, 14)

Based on level flight legs of 20–40 min duration. UT, upper troposphere; MT, middle troposphere; and LT, lower troposphere. $NO_{y_i} = NO_x + PAN + HNO_3$.

*Mean ± 1σ. The numbers in parentheses are the median and the number of data points.

were in good agreement, NO_y data disagreed substantially. The GIT group, using the LIF technique, concluded that their NO_y data should not be used (J. Bradshaw, private communication, 1997). The NO and NO_y data used in this study are from the 30 s measurements obtained by the chemiluminescence instrument from Nagoya University [*Kondo et al.*, 1997b]. This instrument has been tested extensively and found to be minimally impacted by interferences from species such as HCN (2%–5%). Accuracies of the NO and NO_y measurements have been estimated to be 12% and 13%, respectively. Similarly, PAN was measured by electron capture gas chromatography with an accuracy of ±20% [*Singh et al.*, 1996]. HNO_3 was measured using the mist chamber technique with an estimated overall uncertainty of ±35% [*Talbot et al.*, 1997]. NO_2 was not directly measured during PEM-W B. It was calculated from NO using the photochemical model described by *Crawford et al.* [1996]. NO_x is therefore the sum of measured NO and calculated NO_2. Although measured and calculated NO_2 have differed substantially in the past [e.g., *Crawford et al.*, 1996, and references therein], recent improved measurements made during PEM-Tropics A show good agreement between the measured and model-calculated NO_2 concentrations (e.g., J. Bradshaw et al., Photostationary state analysis of the NO_2-NO system based on airborne observations during PEM-Tropics, submitted to *Journal of Geophysical Research*, 1998). We note that in the upper troposphere, only a small fraction (20%–30%) of daytime NO_x is present as NO_2; nevertheless, some uncertainty in the NO_x data should be expected.

All PEM-W B data were archived in a central location, and a variety of merged data files (30–300 s time resolution) were created to provide the best time overlap among the many species that were measured. The most highly time-resolved merged files (i.e., 30 s) were used when possible. The atmosphere sampled during PEM-W B was divided into three regions representing the upper troposphere (UT; 6–12 km), the middle troposphere (MT; 3–6 km), and the lower troposphere (LT; 0–3 km). Latitudinal cross sections of trace species and relevant meteorological parameters were constructed by averaging all data within 5° latitude bins for these altitude regions. About 200 data points for UT and 100 points for MT were averaged per bin. Data strongly influenced by stratospheric air (O_3 > 100 ppb and dew point < −60°C) were excluded to restrict this analysis to the troposphere. Stratospheric data collected during PEM-W B have been discussed elsewhere [*Singh et al.*, 1997]. The latitudinal cross sections are based on airborne measurements performed over a wide area extending from 115° to 160°E over the Pacific. To assess better the nature of the partitioning and budget of reactive nitrogen, we have also evaluated aggregated data for UT, MT, and LT within two latitudinal bins of 30°–45°N (midlatitude) and 10°–30°N (subtropical) and for level legs of 20–40 min duration (Table 1).

Measured latitudinal cross sections are compared with those available from the Harvard global three-dimensional (3-D) model of tropospheric chemistry for a northern hemispheric winter climatology (December/January/February). The Harvard model has a spatial resolution of 4° × 5° with nine vertical layers extending from the surface to 10 mbar and a temporal resolution of 4 hours. Meteorological fields are obtained from the NASA Goddard Institute for Space Studies (GISS) general circulation model (GCM) II. The present version of the model transports 15 reactive chemical tracers: odd oxygen, NO_x, N_2O_5, HNO_4, PANs, alkyl nitrates, HNO_3, CO, ethane, higher alkanes, alkenes, isoprene, acetone, higher ketones, and H_2O_2. Hydrolysis of N_2O_5 to HNO_3 on aerosol surfaces is included with a reaction probability of 0.1. Global sources of NO_x (Tg N yr^{-1}) in the model include 21 from fossil fuel combustion, 0.46 from subsonic aircraft, 11.6 from biomass burning, and 6.6 from soils. A lightning source of 4 Tg N yr^{-1} is apportioned over convective regions following *Price and Rind* [1994]. The amount of NO_y transported from the stratosphere is 0.5 Tg N yr^{-1}. In sum, the total NO_y source in the troposphere is 44 Tg N yr^{-1}. Details of this model, including its structure and validation, are presented by *Wang et al.* [1998a, b]. Latitudinal distributions of selected chemical species for the average winter season were retrieved from this model for the longitudinal band of 130°–150°E. This longitudinal band was considered most representative of the geographical area sampled in PEM-W B. The model output was used from levels that represented averages between 7.4–10.3 km (9 km run) and 2.8–7.3 km (5 km run) and are assumed to correspond to the PEM-W (B) UT and MT, respectively. The model output was also studied for the longitude 115°–130°E for exploratory purposes.

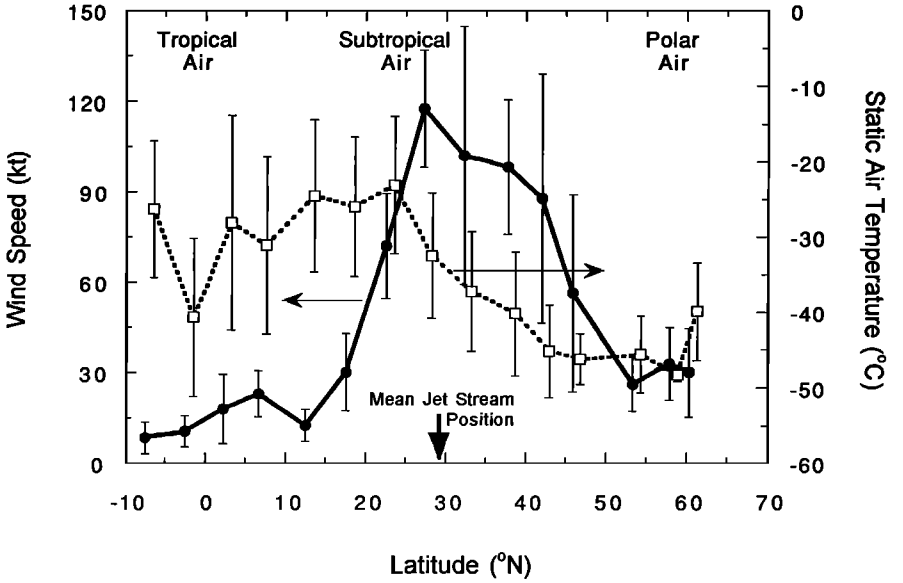

Figure 1. Mean latitudinal distribution of wind speed (solid circle) and static air temperature (SAT) (open square) based on data from the upper troposphere (UT) as collected during Pacific Exploratory Mission-West (PEM-W) B. The wind speed profile identifies the polar jetstream separating polar air from subtropical and tropical air. Latitudinal cross sections here and in subsequent figures were constructed by averaging all tropospheric data within 5° latitude bins. Data points of the two distribution curves have been shifted by 1° in latitude for clarity. In this and all subsequent figures, error bars represent $\pm 1\sigma$, the upper troposphere (6–12 km) is denoted as UT, the middle troposphere (3–6 km) is denoted as MT, and the lower troposphere (0–3 km) is denoted as LT.

3. Results and Discussion

3.1. Transport

Figure 1 shows the cross section for the aircraft-measured wind speed and static air temperature (SAT) for the UT. To show standard deviations as clearly as possible in Figure 1 (and elsewhere in this paper), data points of the two distribution curves have been shifted by 1° with respect to latitude. The polar jetstream separating the relatively cold polar air to the north and the warm subtropical and tropical air to the south is clearly outlined. The jetstream coincides with the area of large temperature gradient (baroclinic zone) between 25° and 40°N. This baroclinic zone was also present at the same location in the middle troposphere from 700 to 500 mbar. It generally identifies the latitude region where strong 3-D tropospheric circulations associated with extratropical cyclones are present. The heavy arrow in Figure 1 indicates the average position (29°N) of the jetstream obtained from the PEM-W B meteorological analyses. The core of the jetstream was at ~200 mbar (≈12 km). Isentropic trajectories computed by *Merrill et al.* [1997] indicated that UT air parcels from 25°N to 45°N were associated with westerly (270°) wind directions with transport from the Asian continent across Japan ("continental north"). At latitudes below 25°N, UT air parcels generally originated from the southeast Asian continent ("continental south"). These trajectories also showed that at 45°N, air parcels originated from a location north of the Arctic circle over the Arctic Ocean near the island of Nova Sembla (75°N, 80°E) 5 days earlier.

3.2. Reactive Nitrogen Species

Figure 2 presents the average ($\pm 1\sigma$) UT and MT latitude distributions of NO, NO_x, PAN, HNO_3, and NO_y. NO data presented here were restricted to solar zenith angles <70° to minimize the effects of diurnal variations. In general, variabilities in Figure 2 are largest in the latitude region of 20°–35°N which represents the core region of the jetstream (Figure 1). These reflect the large variations in atmospheric circulations in this region caused by the migratory midlatitude synoptic-scale storm systems that are closely tied to the polar jetstream. NO makes up a high fraction of NO_x in the low-temperature environment of UT ($NO/NO_x = 0.75 \pm 0.09$) but decreases rapidly with decreasing altitude ($NO/NO_x = 0.42 \pm 0.10$ in MT). In the UT region (Figure 2a), high average NO_x concentrations (75–100 ppt) are present between 20° and 30°N near the center of the jetstream. Individual (30 s average) NO measurements as high as 300–350 ppt were recorded, and significant variability was observed. *Koike et al.* [1997] have suggested that this sampling area is downwind of a busy commercial air corridor between Japan and southeast Asia, and aircraft emissions may have affected the NO measurements. The indicated high NO_x could also be associated with processes involving wet continental convection with associated lightning and long-range transport. Lack of a coincident HNO_3 signature in the UT (Figure 2b) suggests that either HNO_3 was washed out during convection or NO_x was too fresh to have undergone oxidation to HNO_3. The relatively high UT NO (also NO_x) concentrations south of the equator are attributed to lightning. Weather satellites observed large clusters of cumulonimbus clouds south of the equator, and lightning data from satellites showed a maximum frequency during February 1994. Individual NO peaks of 800–900 ppt (10 s data) were often observed [*Kawakami et al.*, 1997]. A coincident HNO_3 and NO_y increase (Figure 2b) was evident in this instance. A similar lightning NO signature was not observed in the MT

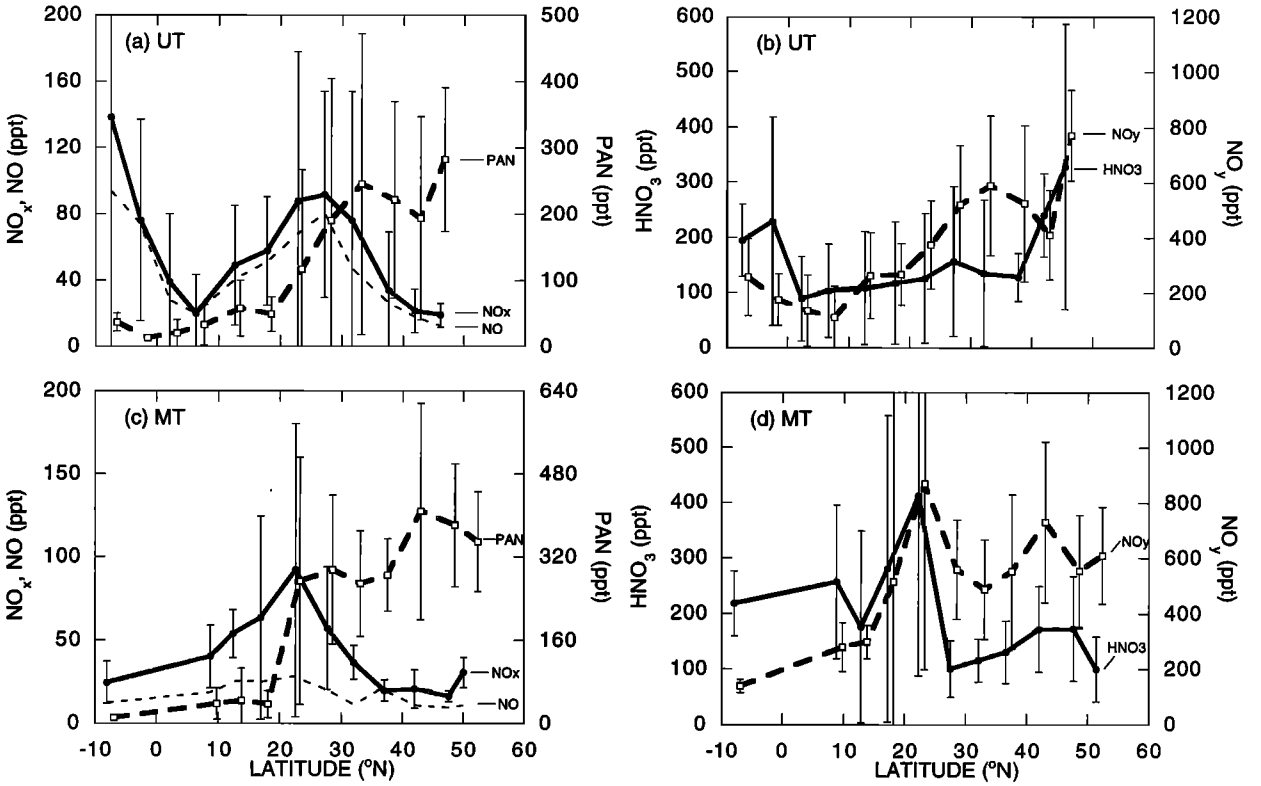

Figure 2. Mean latitudinal distribution of NO, NO_x, peroxyacetylnitrate (PAN), HNO_3, and NO_y in the (a) and (b) UT and (c) and (d) MT. For clarity, data points of the heavy dashed distribution curves (PAN and NO_y) have been shifted by 1° in latitude with respect to the NO_x, NO, and HNO_3 curves.

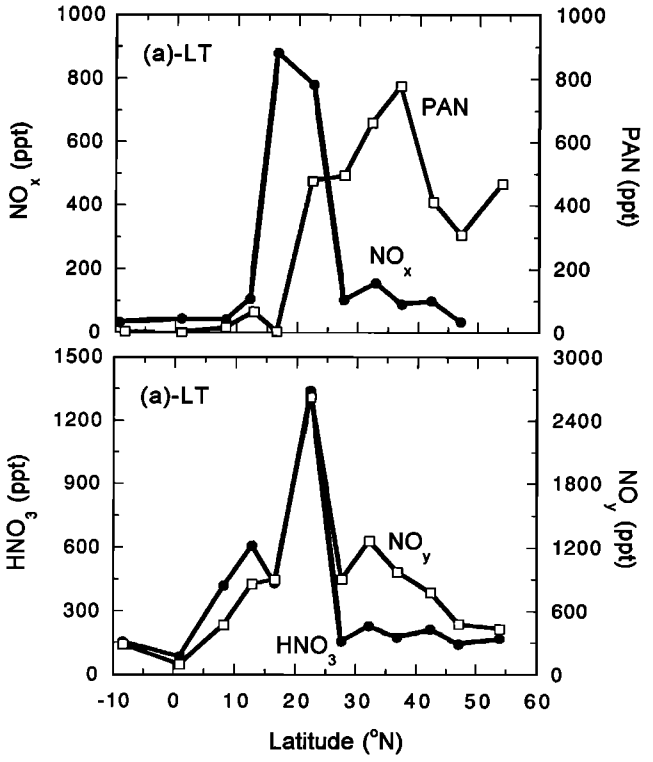

Figure 3. Mean latitudinal distribution of NO_x, PAN, HNO_3, and NO_y in the LT.

region (Figure 2c). The MT NO_x peak around 20°N was generally associated with significant continental pollution signatures that included high HNO_3 and NO_y (Figure 2d). On the polar side of the jetstream, average NO_x concentrations decreased rapidly at all altitude regions. Coincident with this decline were increases in reservoir species as indicated by high PAN and NO_y mixing ratios. Figure 3 shows the mean distribution of these reactive nitrogen species for the LT. The strongest features associated with Asian continental outflow around 20°–25°N are evident. Under these conditions, nearly half of the NO_y was present as HNO_3. Even in the UT, PAN was strongly correlated (R^2 = 0.7–0.8) with tracers of anthropogenic origin (e.g., CO and C_2H_2). *Moxim et al.* [1996] show that midlatitude storm systems can transport PAN (and supposedly other pollutants) poleward and upward from the surface combustion emission regions into the upper tropospheric westerlies.

3.3. Chemical Tracers

To facilitate further data interpretation, we show the mean latitudinal distribution of a number of anthropogenic tracer species for the UT, MT, and LT in Figure 4. These tracer profiles clearly show that most of the sources of these pollutants are located in the industrial northern hemisphere (NH), and their concentrations decline rapidly toward the tropics. The two ratios of C_2H_2/CO and ln (C_3H_8/C_2H_6), independently proposed by *Smyth et al.* [1996] and *Koike et al.* [1997] as indicators of air mass processing and age, further suggest that in the NH, even UT air masses are processed to a much lesser

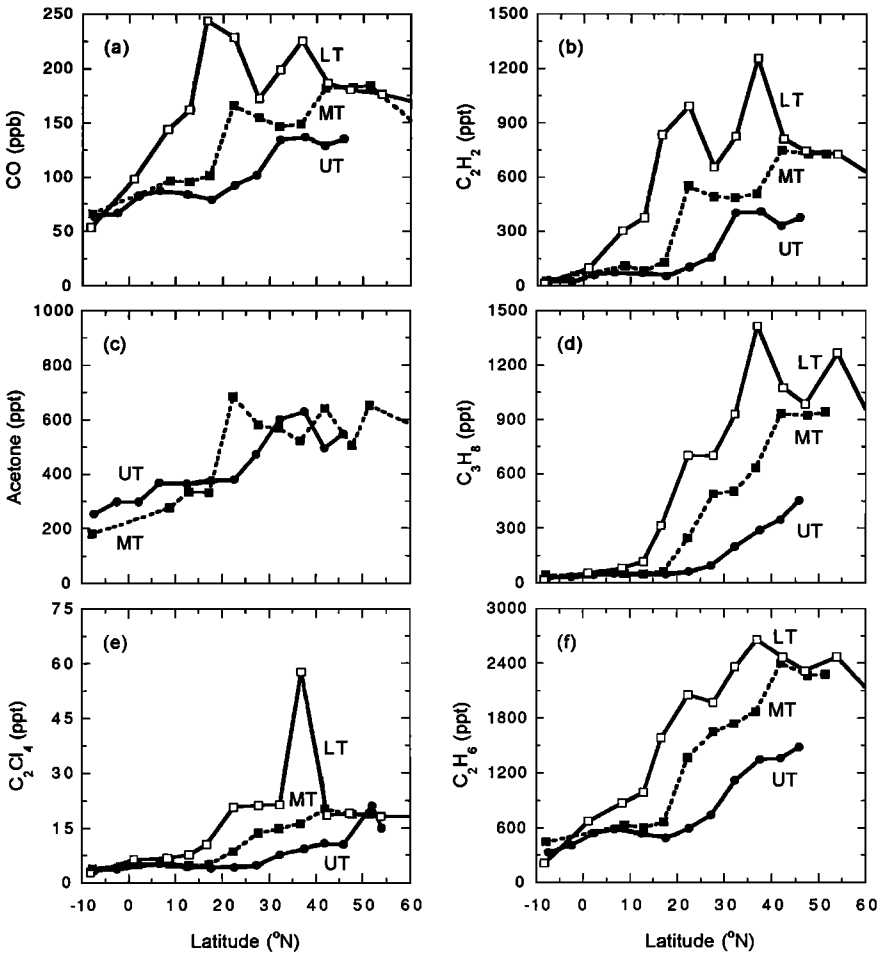

Figure 4. Mean latitudinal distributions of select tracer species for the UT (solid circle), MT (solid square), and LT (open square).

extent than in the tropics and southern hemisphere (SH) (Figure 5). For nearly all cases in Figure 4 a strong gradient of concentrations from the LT to UT, indicative of anthropogenic pollutants with surface level sources, was present. The Asian continental outflow impact near 20°N is clearly evident in the LT-MT measurements (e.g., Figure 4a and 4b) but is greatly moderated in the UT. Trajectory analysis [*Merrill et al.*, 1997] shows that the double maxima in CO and C_2H_2 (tracers of combustion) are associated with Asian outflow at the latitudes of Japan (continental north) and China/southeast Asia (continental south), the latter showing little enhancement in C_2Cl_4 (Figure 4e), a synthetic organic chemical commonly used in highly industrialized nations. The Asian outflow characteristics for continental north and continental south regimes have been discussed in more detail by *Gregory et al.* [1997] and *Talbot et al.* [1997]. Because of excessive moisture interference in the LT, acetone (CH_3COCH_3) was measured only in the UT/MT regions (Figure 4c). The latitudinal distribution of acetone is different from other anthropogenic tracer species, in part because of its diverse but poorly characterized sources. Acetone has been proposed as a major source of PAN and HO_x in the UT [*Singh et al.*, 1995; *Arnold et al.*, 1997; *Wennberg et al.*, 1998].

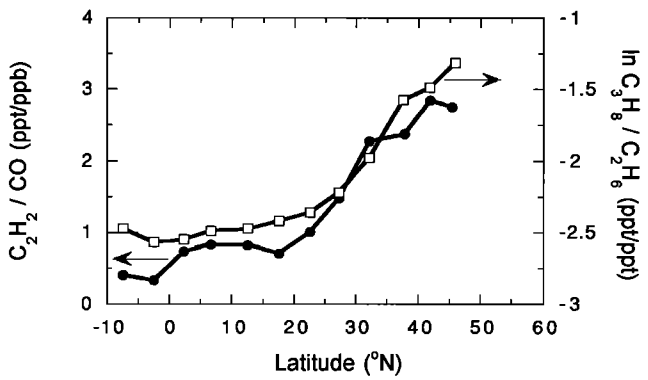

Figure 5. Latitudinal distribution of indices of photochemical processing as represented by C_2H_2/CO and ln (C_3H_8/C_2H_6) ratios for the UT region. Both indices suggest a "young" air mass in the northern latitude region of large industrial pollutant emissions.

3.4. Data-Model Comparisons

Figures 6 and 7 present measured and modeled mean latitudinal distributions of NO, NO_x, PAN, HNO_3, and O_3 for the UT and MT. Similar results for NO_y are presented in Figure 8. While such comparisons are instructive, perfect agreement should not be expected as measurements were often geographically selective and affected by specific weather conditions that prevailed during the late winter/early spring of 1994. The

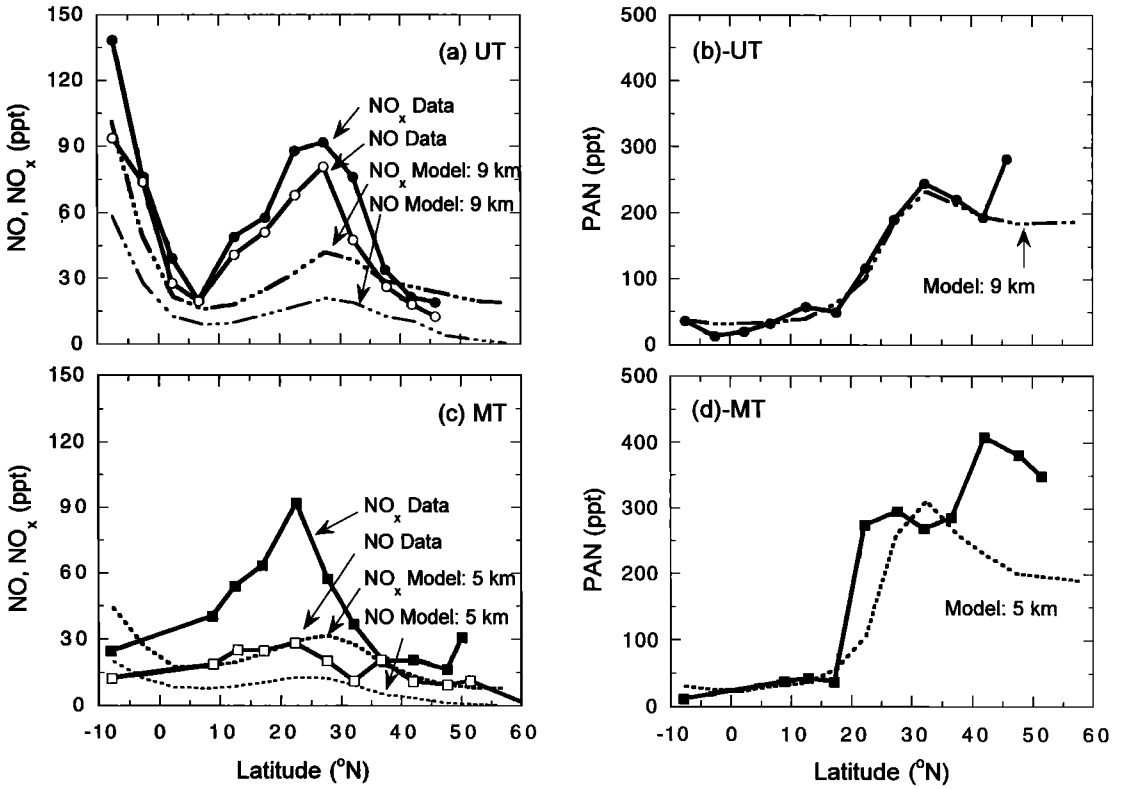

Figure 6. Mean measured and modeled latitudinal distributions of NO, NO_x, and PAN for the UT and MT. The model results in this and subsequent figures are computed for the longitudinal area of 130°–150°E and for a northern hemispheric winter season (December/January/February). The model levels are averaged for 7.4–10.3 km (9 km run) and 2.8–7.3 km (5 km run) and are assumed to correspond to the UT and MT measurements, respectively.

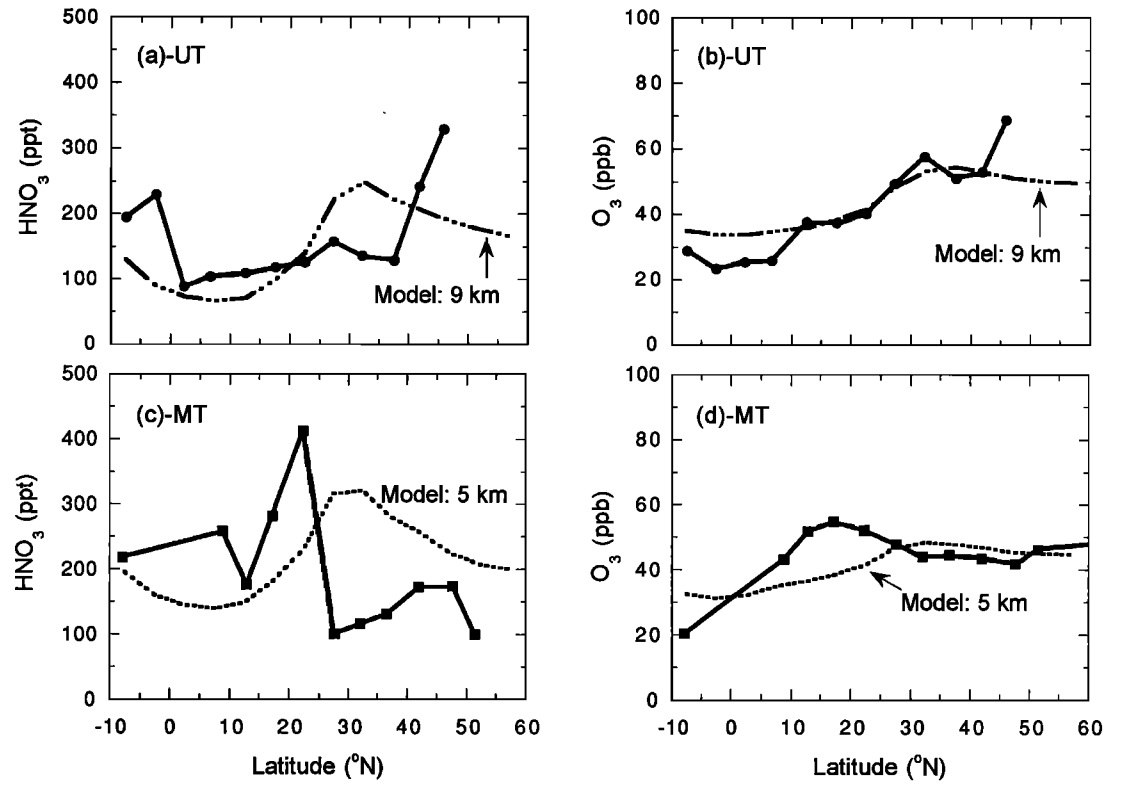

Figure 7. Mean measured and modeled latitudinal distributions of HNO_3 and O_3 for the UT and MT.

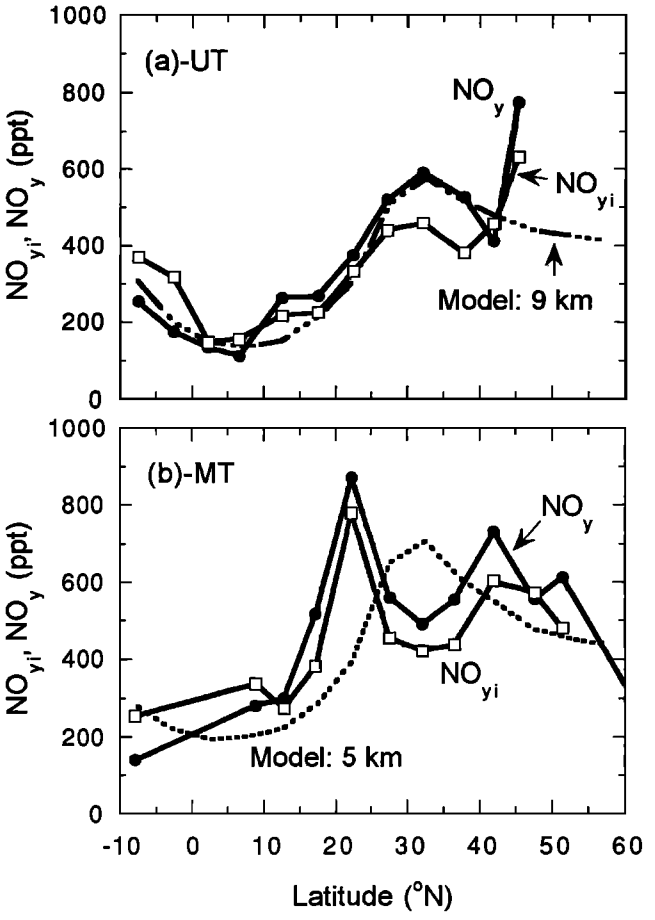

Figure 8. Latitudinal distributions of mean measured NO_y and NO_{yi} and modeled NO_y for the UT and MT. NO_y is directly measured and represents total available reactive nitrogen. NO_{yi} is the sum of NO_x + PAN + HNO_3. Modeled NO_y (dashed lines) is computed from the sum of all reactive nitrogen species included in the model.

model, on the other hand, reflects conditions of atmospheric circulation and chemistry during a typical northern hemispheric winter season. In general, the UT environment should be better represented in the model because it is less impacted by episodic events and more by relatively long-term mixing and transport. For the UT region, there, indeed, is good general agreement between PEM-W B measured and model-predicted PAN, NO_y, and O_3 but less so for HNO_3 and NO (or NO_x). NO_x in the subtropics is significantly underpredicted by the model, most likely because the convective outflow/lightning source from the Asian continent is underestimated in this climatology. Trajectory analysis indicated that the deviation (increase) at ~45°–50°N observed in PAN, HNO_3, NO_y and O_3 was largely due to sampling of polluted air parcels (high CO and NMHCs) that originated from a location north of the Arctic circle. It is also evident that the model captures the south of the equator UT NO (also NO_x) lightning increase well (Figure 6a).

An important feature in Figure 7a is the comparison between measured and model-predicted UT HNO_3. In previous studies, UT model-predicted HNO_3 have exceeded measurements by as much as factors of 10 [*Singh et al.*, 1996; *Jacob et al.*, 1996; A. N. Thakur et al., Distribution of reactive nitrogen species in the remote free troposphere: Data and model comparisons, submitted to *Atmospheric Environment*, 1997, hereinafter referred to as Thakur et al., submitted manuscript, 1997]. Such large disagreements have been used as an argument for the presence of mechanisms to rapidly recycle or remove HNO_3 via heterogeneous chemical mechanisms [*Fan et al.*, 1994; *Chatfield*, 1994; *Hauglustaine et al.*, 1996; *Dentner et al.*, 1996; *Larry et al.*, 1997; A. Tabazadeh et al., HNO_3 scavenging by mineral and biomass aerosols, submitted to *Nature*, 1998, hereinafter referred to as Tabazadeh et al., submitted manuscript, 1998]. The UT comparison between measured and calculated HNO_3 here is within a factor of 2 with no systematic hemispheric asymmetry. Here the predicted HNO_3 is generally below measured values, and there is little obvious need to invoke particle reactions as a means of removing HNO_3. The notion that models significantly overpredict the UT HNO_3, where heterogeneous chemistry may be most effective because of low temperatures and high aerosol acidity, needs to be reassessed. It is noted that gas/particle reactions may be minimized in the UT during winter/early spring because of reduced deep convection resulting in fewer particles. A possible interpretation of these results is that HNO_3 removal by particles is highly seasonal with potentially significant impact only during summer months when particle concentrations may be high (Thakur et al., submitted manuscript, 1997; Tabazadeh et al., submitted manuscript, 1998).

The MT comparisons (Figures 6c, 6d, 7c, and 7d) show larger differences than the UT, most likely because the MT (and even more the LT) begins to reflect the effects of deviations from the model wintertime climatology, i.e., the absence of episodes and weather conditions relevant to the 1994 late winter/early spring. In fact, the HNO_3 and O_3 measurements start to show the significant impact from Asian outflow near 20°N.

3.5. Ratios of Reactive Nitrogen Species

Figure 9 shows modeled and data-derived latitudinal distributions for NO_y/NO_x, HNO_3/NO_x, PAN/NO_x, and NO_y/O_3 ratios for the UT. The observed tendencies of latitudinal behavior of these ratios is generally captured by the model except at 40°–50°N where trajectory analysis showed that polluted air (high CO and NMHCs) from high latitudes was sampled. There is no consistent hemispheric asymmetry in the data versus the modeled HNO_3/NO_x ratio (Figure 9b). The agreement between data and model is substantially better than has been reported in the past [*Liu et al.*, 1992; *Chatfield*, 1994]. The deviations at 10°–30°N are largely attributable to the underprediction of NO_x. The NO_y/O_3 ratio reported by *Murphy et al.* [1993] and by *Folkins et al.* [1995] during two January DC-8 flights from California to Tahiti are in good agreement with Figure 9d. However, the level of agreement between data and modeled NO_y/NO_x ratios seen in Figure 9 is significantly better than that achieved by *Folkins et al.* [1995]. It is also evident that most of the NO_y at northern latitudes resides in reservoir species such as PAN and HNO_3. The presence of chemicals such as acetone in the UT and hydrocarbons in the lower troposphere allows the conversion of NO_x to PAN at all altitudes. *Singh et al.* [1995] use a 3-D model to calculate that 35–45 ppt of PAN in the UT (30°–50°N) could have come from acetone alone. Even higher PAN/NO_x ratios have been reported from northerly latitudes of Alaska and Greenland [*Singh et al.*, 1992]. Once formed, PAN acts as a stable reservoir of NO_x in the UT. Reservoir species such as PAN also

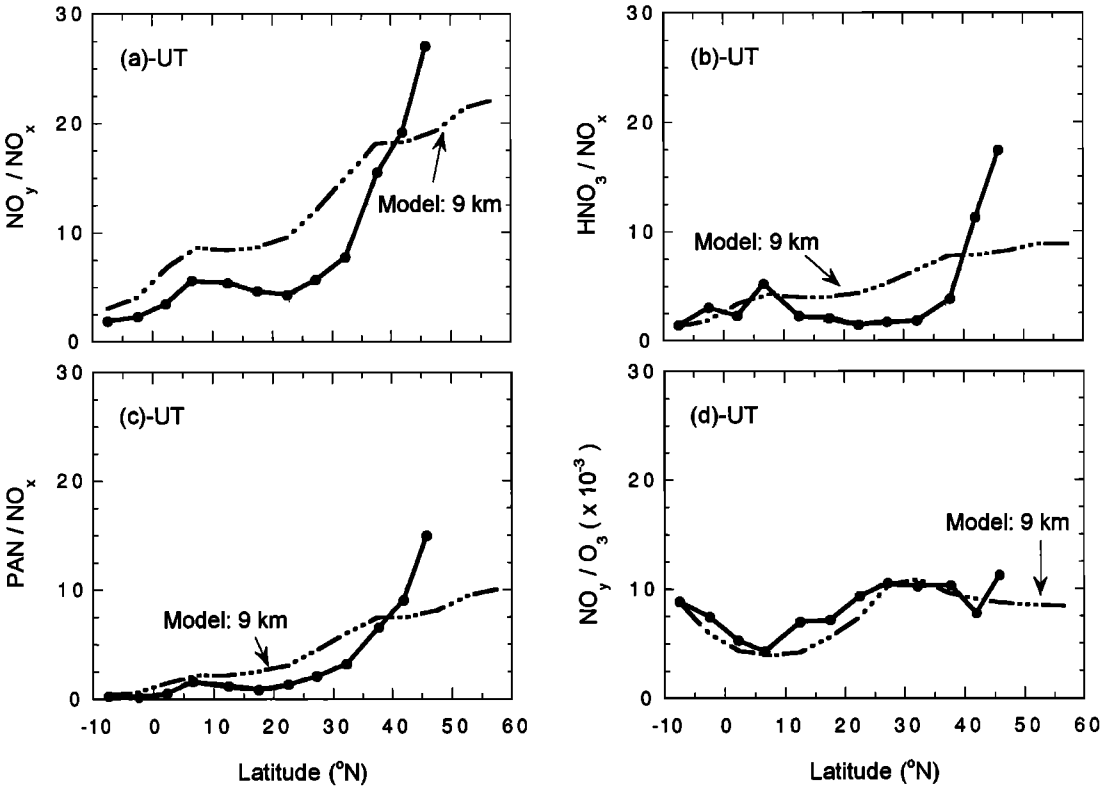

Figure 9. Mean latitudinal distributions of NO_y/NO_x, HNO_3/NO_x, PAN/NO_x and NO_y/O_3 ratios for the UT based on measurements and model predictions. All ratios are expressed as ppt ppt^{-1}.

prevent the accumulation of large quantities of NO_x. *Kanakidou et al.* [1991] calculated that PAN formation from C_2H_6 and C_3H_8 chemistry alone reduces NO_x mixing ratios by nearly 30% during winter in the middle and upper troposphere of the NH. Atmospheric circulations known to be present on the anticyclonic windshear side of the jetstream can carry the reservoir PAN downward and southward to the warm lower troposphere where it can be thermally converted to NO_x to influence regional O_3 photochemistry [*Moxim et al.*, 1996]. In general, the results from Figures 6–9 demonstrate that the latitude distributions observed during PEM-W B reflect to a large extent our present understanding of reactive nitrogen transport and chemistry.

3.6. Partitioning and Budget of Reactive Nitrogen

Figure 8a shows the mean UT latitudinal distribution of measured NO_y. NO_y increases from ~100–200 ppt in the tropics to nearly 700 ppt at northern midlatitudes. The high linear correlation that was found between NO_y and O_3(R^2 = 0.82) and other tracers reflects the fact that NO_y includes the precursors (e.g., NO_x) and products (HNO_3 and PAN) of O_3 photochemistry. Also shown in Figure 8a is the latitudinal distribution of NO_{y_t} (NO_x + HNO_3 + PAN). It is evident that both NO_y and NO_{y_t} have similar tendencies as a function of latitude, and their abundances are in reasonable agreement even though NO_{y_t} is composed of three independent measurements. Further, the model-predicted UT NO_y shows remarkably consistent behavior across all latitudes. The distribution of NO_y and NO_{y_t} in the MT (Figure 8b) is more complex, perhaps because of greater continental influences during the PEM-W B measurement period, but once again, there is excellent internal consistency in these observations. As discussed earlier, the model is unable to fully capture the complex observed structure in the MT in part because of the episodic nature of outflow events, limited sampling, and winter average conditions for the model.

In order to capture the nature of the partitioning and budget of reactive nitrogen in a more quantitative fashion we evaluated aggregated data for UT, MT, and LT within two latitudinal bands of 30°–45°N (midlatitude) and 10°–30°N (subtropical) and only for level legs of 20–40 min duration. Even though this restricted the available data, it provided a robust approach to studying this budget and partitioning involving multiple measurements on different timescales. A strong linear correlation between NO_y and NO_{y_t} (NO_x + PAN + HNO_3) that is independent of latitude can be seen in Figure 10. These partitioning results are further summarized in Table 1. Some 85% of the reactive nitrogen in the UT/MT region is accounted for by NO_x, PAN, and HNO_3. *Thompson et al.* [1997] have used a model to estimate that 10%–20% of reactive nitrogen in the UT may exist in the form of species that were not measured (e.g., alkyl nitrates and HNO_4). The budget of reactive nitrogen thus appears to be reasonably balanced. It is further evident from Table 1 that PAN and HNO_3 dominate the NO_y reservoir while NO_x makes a smaller contribution. These partitioning results are in general agreement with those reported earlier on the basis of an analysis of these data for the troposphere and the stratosphere [*Kondo et al.*, 1997a; *Singh et al.*, 1997]. The reasons for the overall improvement in the reactive nitrogen budget in PEM-W B, compared with previous experiments [*Sandholm et al.*, 1994; *Singh et al.*, 1996], are not ob-

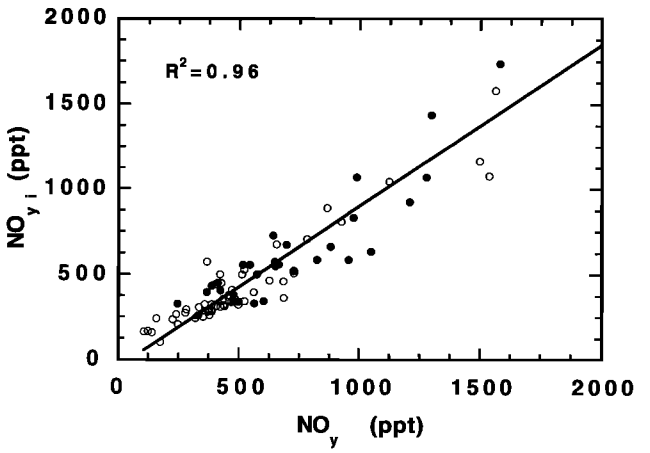

Figure 10. Linear relationship between the sum of measured reactive nitrogen species (NO_{yi} = NO_x + PAN + HNO_3) and measured NO_y on the basis of level flight legs of 20–40 min duration as in Table 1. Data are for all altitudes. Open circles represent measurements at midlatitudes (30°–45°N), and solid circles represent measurements at the subtropics (10°–30°N). [NO_{yi} ppt] = −48.5 + 0.95 [NO_y ppt].

vious but may reflect improvements in instrument performance and accuracy.

4. Conclusions

The 1994 late winter/early spring measurements of PEM-W B over the western Pacific Ocean have been analyzed to show latitude distributions of the concentrations of selected reactive nitrogen species and chemical tracers. The mixing ratios are relatively low in the warm tropical and subtropical air south of the polar jetstream but increase sharply with latitude toward the cold polar air north of the jetstream. The exception is NO_x which decreases from the tropics toward midlatitudes. The NO_x at the high latitudes, however, is likely sequestered in reservoir species like PAN and its homologues. Atmospheric circulations known to be present on the anticyclonic windshear side of the jetstream can carry the PAN reservoir downward and southward to the warm lower troposphere where it can be thermally converted to NO_x to influence regional O_3 photochemistry. Comparisons with the Harvard global 3-D model of tropospheric chemistry suggest that PEM-W B measurements from the upper troposphere were generally consistent with the present state of knowledge. Nearly 85% of the total reactive nitrogen (NO_y) could be accounted for by NO_x, PAN, and HNO_3 alone. It has been estimated that known but unmeasured species may account for the remainder. Improved comparison between HNO_3 observations and theory, compared to previous studies, suggests that rapid recycling of HNO_3 via unknown heterogeneous processes to NO_x may be less effective than previously suggested. However, it is possible that such recycling processes could be important in some regions and not in others [*Wang et al.*, 1998b].

Acknowledgment. This research was supported by the NASA Global Tropospheric Experiment. We acknowledge all PEM-W B participants for their cooperation and support. Special thanks are due to the DC-8 flight and ground crew of the NASA Ames Research Center for making the experiment a success. D. J. Jacob and Y. Wang acknowledge support from the NASA Atmospheric Chemistry and Modeling Program.

References

Arnold, F., V. Burger, B. Droste-Fanke, F. Grimm, A. Krieger, J. Schneider, and T. Stilp, Acetone in the upper troposphere and lower stratosphere: Impact on trace gases and aerosols, *Geophys Res. Lett.*, *24*, 3017–3020, 1997.

Chatfield, R. B., Anomalous HNO_3/NO_x ratio of remote tropospheric air: Conversion of nitric acid to formic acid and NO_x, *Geophys. Res. Lett.*, *21*, 2705–2708, 1994.

Crawford, J., et al., A photostationary state analysis of the NO_2-NO system based on airborne observations from the western and central North Pacific, *J. Geophys. Res.*, *101*, 2053–2072, 1996.

Dentner, F. J., G. R. Carmichael, Y. Zhang, J. Lelieveld, and P. J. Crutzen, Role of mineral aerosol as a reactive surface in the global troposphere, *J. Geophys. Res.*, *101*, 22,869–22,879, 1996.

Fan S.-M., et al., Origin of tropospheric NO_x over subarctic eastern Canada in summer, *J. Geophys. Res.*, *99*, 16,867–16,877, 1994.

Folkins, I. A., et al., O_3, NO_y, and NO_x/NO_y in the upper troposphere of the equatorial Pacific, *J. Geophys. Res.*, *100*, 20,913–20,926, 1995.

Gregory, G. L., J. T. Merrill, M. C. Shipham, D. R. Blake, G. W. Sachse, and H. B. Singh, Chemical characteristics of tropospheric air over the Pacific Ocean as measured during PEM-West B: Relationship to Asian outflow and trajectory history, *J. Geophys. Res.*, *102*, 28,275–28,285, 1997.

Hauglustaine, D. A., B. A. Ridley, S. Solomon, P. G. Hess, and S. Madronich, HNO_3/NO_x ratio in the remote troposphere during MLOPEX 2: Evidence for nitric acid reduction on carbonaceous aerosol, *Geophys. Res. Lett.*, *23*, 2609–2613, 1996.

Hoell, J. M., et al., The Pacific Exploratory Mission-West Phase B: February–March, 1994, *J. Geophys. Res.*, *102*, 28,223–28,239, 1997.

Jacob, D. J., et al., Origin of ozone and NO_x in the tropical troposphere: A photochemical analysis of aircraft observations over the South Atlantic basin, *J. Geophys. Res.*, *101*, 24,235–24,250, 1996.

Kanakidou, M., H. B. Singh, K. M. Valentin, and P. J. Crutzen, A 2-D model study of ethane and propane oxidation in the troposphere, *J. Geophys. Res.*, *96*, 15,395–15,413, 1991.

Kawakami, M., et al., Impact of lightning and convection on the tropical free troposphere, *J Geophys. Res.*, *102*, 28,367–28,384, 1997.

Koike, M., et al., Reactive nitrogen and its correlation with O_3 and CO over the Pacific in winter and early spring, *J. Geophys Res.*, *102*, 28,285–28,404, 1997.

Kondo, Y., et al., Profiles and partitioning of reactive nitrogen over the Pacific Ocean in winter and early spring, *J. Geophys Res.*, *102*, 28,405–28,424, 1997a.

Kondo, Y., S. Kawakami, M. Koike, D. W. Fahey, H. Nakajima, Y. Zhao, and N. Toriyama, The performance of an aircraft instrument for the measurement of NO_y, *J. Geophys. Res.*, *102*, 28,663–28,671, 1997b.

Larry, D. J., A. M. Lee, R. Toumi, M. J. Newchurch, M. Pirre, and J. B. Renard., Carbon aerosols and atmospheric photochemistry, *J. Geophys Res.*, *102*, 3671–3682, 1997.

Liu, S. C., et al., A study of the photochemistry and ozone budget during the Mauna Loa Observatory Photochemistry Experiment, *J. Geophys. Res.*, *97*, 10,463–10,471, 1992.

Merrill, J. T., R. Newell, and A. S. Bachmeier, A meteorological overview for the Pacific Exploratory Mission-West Phase B, *J Geophys. Res.*, *102*, 28,241–28,253, 1997.

Moxim, W. J., H. Levy II, and P. S. Kasibhatla, Simulated global tropospheric PAN: Its transport and impact on NO_x, *J. Geophys. Res.*, *101*, 12,621–12,638, 1996.

Murphy, D. M., D. W. Fahey, M. H. Proffitt, S. C. Liu, K. R. Chan, C. S. Eubank, S. R. Kawa, and K. K. Kelly, Reactive nitrogen and its correlation with ozone in the lower stratosphere and upper troposphere, *J. Geophys. Res.*, *98*, 8751–8773, 1993.

Price, C., and D. Rind, Modeling global lightning distributions in a general circulation model, *Mon. Weather Rev.*, *122*, 1930–1939, 1994.

Sandholm, S., et al., Summertime partitioning and budget of NO_y compounds in the troposphere over Alaska and Canada: ABLE 3B, *J. Geophys. Res.*, *99*, 1837–1861, 1994.

Singh, H. B., et al., Relationship of PAN to active and total odd nitrogen at northern high latitudes: Influence of reservoir species on NO_x and O_3, *J. Geophys. Res.*, *97*, 16,523–16,530, 1992.

Singh, H. B., M. Kanakidou, P. J. Crutzen, and D. J. Jacob, High

concentrations and photochemical fate of oxygenated hydrocarbons in the global troposphere, *Nature*, *378*, 50–54, 1995.

Singh, H. B., et al., Reactive nitrogen and ozone over the western Pacific: Distribution, partitioning, and sources, *J. Geophys. Res.*, *101*, 1793–1808, 1996.

Singh, H. B., Y. Chen, G. L. Gregory, G. W. Sachse, R. Talbot, D. R. Blake, Y. Kondo, J. D. Bradshaw, B. Heikes, and D. Thornton, Trace chemical measurements from the northern midlatitude lowermost stratosphere in early spring: Distributions, correlations, and fate, *Geophys. Res. Lett.*, *24*, 127–130, 1997.

Smyth, S., et al., Comparison of free tropospheric western Pacific air mass classification schemes for the PEM-West A experiment, *J. Geophys. Res.*, *101*, 1743–1762, 1996.

Talbot, R. W., et al., Chemical characteristics of continental outflow from Asia to the troposphere over the western Pacific Ocean during February–March 1994: Results from PEM-West B, *J. Geophys. Res.*, *102*, 28,255–28,274, 1997.

Thompson, A. M., H. B. Singh, R. W. Stewart, and T. L. Kucsera, A Monte Carlo study of upper tropospheric reactive nitrogen on PEM-West B, *J. Geophys. Res.*, *102*, 28,437–28,446, 1997.

Wang, Y., D. J. Jacob, and J. A. Logan, Global simulation of tropospheric O_3-NO_x-hydrocarbon chemistry, 1, Model formulation, *J. Geophys. Res.*, *103*, 10,713–10,725, 1998a.

Wang, Y., J. A. Logan, and D. J. Jacob, Global simulation of tropospheric O_3-NO_x-hydrocarbon chemistry, 2, Model evaluation and global ozone budget, *J. Geophys. Res.*, *103*, 10,727–10,755, 1998b.

Wennberg, P. O., et al., Hydrogen radicals, nitrogen radicals, and the production of ozone in the upper troposphere, *Science*, *279*, 49–53, 1998.

D. R. Blake, Department of Chemistry, University of California, Irvine, CA 92717.

Y. Chen, H. B. Singh, A. N. Thakur, and W. Viezee, Earth Science Division, NASA Ames Research Center, Moffett Field, CA 94035. (e-mail: hsingh@mail.arc.nasa.gov)

G. L. Gregory and G. W. Sachse, Earth Science Division, NASA Langley Research Center, Hampton, VA 23665.

D. J. Jacobs and Y. Wang, Department of Earth and Planetary Sciences, Harvard University, Cambridge, MA 02139.

Y. Kondo, Solar Terrestrial Environment Laboratory, Nagoya University, Honohara 3-13, Toyokawa, Aichi 442, Japan.

R. W. Talbot, Institute for the Study of Earth, Oceans, and Space, University of New Hampshire, Durham, NH 03824.

(Received April 22, 1997; revised May 21, 1998;
accepted May 29, 1998.)